

Decelerating Plasmoid Model for Gamma-Ray Burst Afterglows

James Chiang¹ & Charles D. Dermer

E. O. Hulburt Center for Space Research, Code 7653,
Naval Research Laboratory, Washington, DC 20375-5352

ABSTRACT

The flaring and fading radio, optical, and X-ray afterglows from GRB 970508 are modeled by a highly relativistic plasma sphere which decelerates by sweeping up ambient gas. The afterglow emission is assumed to be synchrotron radiation emitted by nonthermal electrons in the magnetized plasmoid. The temporal behavior of the delayed emission is controlled by the evolution of the Doppler factor and by adiabatic expansion losses of the nonthermal electrons in the plasmoid. Model fits to the optical data of GRB 970508 are provided, and the relative delay of the radio peak to the optical peak is found to result from a decrease in the observed self-absorption frequency as the plasmoid expands and decelerates. A variety of afterglow behaviors occurs for different observing angles and plasmoid parameters. The degree of collimation inferred from our fit to GRB 970508 implies a space density of GRB sources which exceeds the estimates from scenarios involving coalescing compact objects. This model can be verified through observations of superluminal motion in the delayed radio emission.

Subject headings: gamma rays: bursts — radiation mechanisms: nonthermal

1. Introduction

Beppo-SAX observations (Heise 1997) of fading X-ray emission have resulted in the first identified radio and optical counterparts to gamma-ray bursts (GRBs). Five GRBs have been localized with the Wide Field Camera of the Beppo-SAX experiment to within 3 arc minutes (one during the science verification phase), with 3 showing X-ray afterglows. Optical counterparts have been identified for GRB 970228 and GRB 970508, with a flaring radio counterpart identified with the latter GRB (Frail et al. 1997). Detection of optical Fe II and Mg II absorption lines in the spectrum of the optical counterpart to GRB 970508 (Metzger et al. 1997) demonstrates that at least one GRB is at cosmological distances with $z \geq 0.835$. Even though GRB 970111 was the most intense of the five Beppo-SAX bursts, an X-ray afterglow was not detected from it. This indicates that very different behaviors should be expected from different GRBs.

¹NAS/NRC Resident Research Associate

The high energy emission from GRBs is almost certainly radiated by non-thermal particles as evidenced by their rapid variability and broken power-law spectral shapes (e.g., Fishman & Meegan 1995). The spectra of the afterglows also indicate a non-thermal origin. The spectrum of the GRB 970228 afterglow has a flux density $F_\nu \propto \nu^{-1/2}$ extending from the optical to the X-rays (Katz, Piran & Sari 1997). The optical spectrum of the GRB 970508 afterglow measured at May 10.178 UT (30.6 hours after the initial burst at May 8.904 UT) is also a power-law with energy index $\alpha = 0.65$ (Djorgovski et al. 1997). Furthermore, the optical/X-ray spectral index found by interpolating the R-band fluxes at the time of the Beppo-SAX NFI X-ray observation at May 9.1375 UT is consistent with this value. The radio spectrum of GRB 970508 measured on May 13.96 UT rises from 1.43 to 8.46 GHz with index $\alpha \approx -1.1$ ($S_\nu \propto \nu^{-\alpha}$; Frail et al. 1997) which suggests a self-absorbed synchrotron spectrum with self-absorption frequency near 10 GHz. Taken together, these data argue in favor of a nonthermal synchrotron process for the afterglow emission.

The inferred isotropic total energy of GRB 970508 at $z = 0.835$ is $\approx 10^{52}$ ergs (e.g., Waxman 1997), which exceeds the energy available through $\nu\bar{\nu} \rightarrow e^+e^-$ processes in neutron-star coalescence events (Ruffert et al. 1997) by $\gtrsim 3$ orders of magnitude. Blast-wave scenarios involving the impulsive release of energy into a thin, spherically expanding shell also encounter difficulties in explaining the complex time profiles of GRBs under the assumption of local spherical symmetry for the blast wave (Fenimore, Madras & Nayakshin 1996). Relativistic outflows consisting of discrete emitting components relieve the energetics problems and may also ameliorate the difficulties in explaining GRB light curves.

In this *Letter*, we consider a model for GRB afterglows where the emission is produced by nonthermal electrons entrained in collimated, highly relativistic magnetized plasmoids. The initial flaring of the emission at frequencies greater than the self-absorption frequency is due to the opening angle of the beaming cone intercepting the line-of-sight as the plasmoid slows down. At lower frequencies, the light curve is also affected by the evolution of the self-absorption frequency. Subsequent fading of the emission results from bulk deceleration of the plasmoid and the corresponding decrease of the Doppler factor with time. We provide model fits to the optical light curve of GRB 970508 which bracket the delayed radio emission and which are in accord with the measured X-ray emission. If the model parameters used to fit GRB 970508 are representative of a substantial fraction of GRBs, then implications for the number of GRB sources and the nature of the GRB emission mechanism follow.

2. Dynamics and Synchrotron Emission for a Homogeneous Plasma Sphere

For simplicity we approximate the geometry of the emitting plasma as a single, homogeneous sphere, although the afterglow emitting region could have a more complex geometry or be composed of many separate emission elements moving with a range of speeds. Let R_0 be the initial comoving radius of the plasmoid at time t_0^* as measured in the frame of the burst

explosion. If most of the energy content of the plasmoid is contained in a nonrelativistic thermal component and the plasmoid expands adiabatically with thermal speed $v_{\text{th}}(t) = v_{\text{th},0}R_0/R(t)$, then $R(t) = [R_0^2 + 2v_{\text{th},0}R_0t]^{1/2}$, where t is the time measured in the comoving frame of the plasmoid. Conservation of momentum for the plasmoid in the limit of negligible internal energy loss due to radiation (Katz 1994; see Katz and Piran 1997 for the opposite limit) implies that $m(x)\beta(x)\Gamma(x) = m_0\beta_0\Gamma_0$, where $m(x) = m_0 + \int_{x_0}^x dx' \rho(x')A(x')$ is the total mass at location x , $\rho(x)$ is the mass density of ambient gas, and $A[x(t)] = \pi R^2(t)$ is the cross-sectional area of the plasmoid. Here $\Gamma(x)$ is the bulk Lorentz factor of the plasmoid at x , and $\Gamma_0 = \Gamma(x_0)$. The relation between the time elements in the comoving and explosion frame is just $\delta t^* = \Gamma \delta t$. These expressions are solved iteratively to determine the speed of the plasmoid as a function of time.

We assume that nonthermal electrons are described in the comoving frame by an isotropic angular distribution and a power-law shock-acceleration spectrum given by $N_e(\gamma_0) \equiv N_0\gamma_0^{-p}$ for $1 \leq \gamma_0 \leq \gamma_{\text{max}}$, where γ_0 is the injection electron Lorentz factor. These electrons lose energy by adiabatic and synchrotron processes. The adiabatic energy-loss rate for relativistic electrons is given by $-\dot{\gamma}_{\text{adi}} \cong \gamma \dot{V}/(3V) = \gamma \dot{R}/R$. When such losses dominate,

$$N_e[\gamma(t)] = N_0\gamma^{-p} \left[\frac{R(t)}{R_0} \right]^{1-p}, \quad 1 \leq \gamma \leq \gamma_{\text{max}} \frac{R_0}{R(t)}, \quad (1)$$

where $N_0 = E_{\text{nt}}(2-p)/[m_e c^2(\gamma_{\text{max}}^{2-p} - 1)]$ and E_{nt} is the energy injected into the nonthermal electrons.

The optically thin synchrotron flux density is given by

$$S_{\text{syn}}(\epsilon; \Omega) = m_e c^2 \mathcal{D}^{3+\alpha} \frac{N_0 k_{\text{syn}}(p) \epsilon_{\text{B}}}{d_L^2} (1+z)^{1-\alpha} \left(\frac{\epsilon}{\epsilon_{\text{B}}} \right)^{-\alpha}, \quad 1 \lesssim \frac{\epsilon(1+z)}{\mathcal{D} \epsilon_{\text{B}}} \lesssim \gamma_{\text{max}}^2, \quad (2)$$

where $\mathcal{D} = [\Gamma(1 - \beta\mu)]^{-1}$ is the Doppler factor, d_L is the luminosity distance to the source, $\alpha = (p-1)/2$, $\epsilon = h\nu/(m_e c^2)$, $\epsilon_{\text{B}}(t) = B(t)/(4.414 \times 10^{13} \text{ Gauss})$, and $B(t) = B_0 [R_0/R(t)]^{2q}$ with $q = 1$ for flux-freezing. The angle between the beaming axis and the observer is $\theta = \cos^{-1} \mu$, and $k_{\text{syn}}(p) = (3/2)^\alpha a(p) \alpha_f^2 c / (2\pi r_e)$ where α_f is the fine structure constant, r_e is the classical electron radius, and $a(p)$ is a combination of Γ -functions given by Blumenthal & Gould (1970). The self-absorption frequency is

$$\epsilon_m(t) = \frac{\mathcal{D} \epsilon_{\text{B}}}{1+z} \left[\frac{9}{8\pi} \frac{\sigma_T c(p) N_0}{\alpha_f d(p) \epsilon_{\text{B}} R^2} \right]^{2/(p+4)}. \quad (3)$$

Here $c(p)$ is another combination of Γ -functions and $d(p)$ is the optical depth to synchrotron self-absorption through the center of the plasmoid at the self-absorption frequency; both these functions are described and tabulated by Gould (1979). Above and below the self-absorption frequency, the observed spectrum can be well-described by a broken power-law:

$$S_{\text{syn}}(\epsilon; \Omega) = S_0 \left(\frac{\epsilon}{\epsilon_m} \right)^{-\alpha}, \quad \max(\epsilon_{\text{B}}, \epsilon_m) \leq \epsilon \leq \epsilon_{\text{B}} \gamma_{\text{max}}^2 \quad (4)$$

$$= S_0 \left(\frac{\epsilon}{\epsilon_m} \right)^{-5/2}, \quad \epsilon < \epsilon_m, \quad (5)$$

where the normalization S_0 is given by Equation 2. We also calculate the synchrotron self-Compton component (see Dermer, Sturmer, & Schlickeiser 1997) and find that it makes negligible contribution to the radio through X-ray emission of the GRB 970508 afterglow.

3. Model Fits for the GRB 970508 Afterglow Light Curves

The optical afterglow light curve of GRB 970508 was found to rise following the burst event; it then peaked after ~ 2 days, and thereafter decayed with an approximate t_{obs}^{-1} dependence similar to the decay law of the GRB 970228 optical afterglow. The most extensive set of flux measurements for GRB 970508 are in the R-band, for which precise photometric estimates have been made for a subset of these observations (Djorgovski et al. 1997). The R-band data is shown in Figure 1a along with our approximate fits for two sets of burst and plasmoid parameters.

In the context of our decelerating plasmoid model, the shape of the afterglow light curve can be understood analytically by considering the simpler case where the ambient density and plasmoid cross-sectional area are constants. The peak in the optical light curve occurs when the bulk Lorentz factor has decreased to a value of $\Gamma_p \simeq 1/\theta$. Note that if the observing angle $\theta \lesssim 1/\Gamma_0$, then there will be no initial rise in the light curve of the non-self-absorbed emission as observed for the initial optical afterglow of GRB 970228. The ratio $F_{\nu,p}/F_{\nu,0}$ of the peak flux and the flux at early time is proportional to $(\mathcal{D}_p/\mathcal{D}_0)^{3+\alpha}$ (cf. Equation 2), where \mathcal{D}_p and \mathcal{D}_0 are the Doppler factors at the time of the peak flux and immediately following the burst, respectively. For $\Gamma^2 \gg 1$ and $\theta \ll 1$, the Doppler factor is $\mathcal{D} \cong 2\Gamma/(1 + \Gamma^2\theta^2)$ so that the ratio of peak to initial Doppler factor is $\mathcal{D}_p/\mathcal{D}_0 \cong 2\Gamma_0\theta/(1 + \Gamma_0^2\theta^2)$. Using this result and the flux ratio found from the R-band light curve, $F_{\nu,p}/F_{\nu,0} \simeq 4$, we solve for θ and find $\theta \simeq 2.6/\Gamma_0$.

The time delay of the peak, τ_{obs} , constrains the cross-sectional area A_0 of the plasmoid and the density of the ambient medium. From momentum balance, we have $\Gamma_p/\Gamma_0 \cong (1 + A_0\rho c\tau^*/m_0)^{-1}$. This gives

$$A_0 \cong \frac{\Gamma_0\theta - 1}{\Gamma_0} \frac{E_0\theta^2}{2\rho c^3\tau_{\text{obs}}}, \quad (6)$$

where we have used the approximation $\tau_{\text{obs}} \cong \tau^*\theta^2/2$. The expansion of the plasmoid has the effect of increasing the required value of θ and reducing the required initial cross-sectional area of the plasmoid relative to the non-expanding case. All non-self-absorbed emission below the high-energy cutoffs should rise and fall with the same characteristic behavior in this model.

In producing the fits shown in Figure 1a, we have fixed the total plasmoid energy $E_0 = 10^{50}$ ergs (which is dominated by the kinetic energy of the thermal plasma, i.e., $E_0 = \Gamma_0 m_0 c^2$), set $p = 2.3$ in accord with the measured optical spectral index of $\alpha = 0.65$ (Djorgovski et al. 1997), and considered bulk initial Lorentz factors for the plasmoid in the range $\Gamma_0 = 10^2$ – 10^3 . We have also considered initial thermal expansion velocities in the range $v_{\text{th}} = 10^7$ – 3×10^9 cm s $^{-1}$ and ambient densities of $\rho = 0.1$ – 1 cm $^{-3} \times m_p$. The initial energy of nonthermal electrons is determined by

an injection efficiency defined by $\eta \equiv E_{\text{nt}}/E_0$. The complete set of parameters for the two fits is given in Table 1. We note that the magnetic field strengths of the plasmoid in both cases are well below the equipartition values, which ensures that the self-absorption frequency is not too high. Furthermore, we find that these relatively low values for the magnetic field are also consistent with our assumption that the electron spectrum evolves mainly through adiabatic cooling, since synchrotron cooling is only important at frequencies

$$\nu_{\text{obs}} \text{ (Hz)} \gtrsim \frac{3 \times 10^{16}}{(\mathcal{D}/100)(B/0.01 \text{ G})^3(t_{\text{obs}}/10^6 \text{ s})^2}. \quad (7)$$

Just below the self-absorption frequency, expansion of the plasmoid plays an important role in determining the location of the peak of the light curve. For the afterglow of GRB 970508, the peak of the radio emission is delayed by a few days relative to the peak of the optical light curve, and this is consistent with the inference that the self-absorption frequency is in this range. As the plasmoid expands, it becomes non-self-absorbed at increasingly lower frequencies. This produces an additional enhancement in the observed flux at these frequencies superposed on the flaring of the emission due to the deceleration of the plasmoid, which also causes the observed self-absorption frequency to decrease with time. The 8.4–8.46 GHz radio data (Frail et al. 1997) shown in Figure 1b is bracketed by our model results which fit the optical light curve in Figure 1a. The parameters in Table 1 cover a wide range of values and have not been fine-tuned to fit the radio data precisely. However, the model fits pass through the X-ray data point (Piro et al. 1997) shown in Figure 1c without any additional adjustment. Our model predicts that the X-ray and optical light curves would rise and fall together, except that the X-ray flux can also decline as a result of synchrotron cooling (cf. Eq. [7]) or, depending on the initial value of γ_{max} , through either adiabatic or synchrotron losses.

4. Discussion

We have proposed a model for GRB afterglows where nonthermal electrons emit synchrotron radiation in relativistic bulk plasma outflows. Other models for GRB afterglows also consider synchrotron processes (e.g., Wijers, Rees, & Mészáros 1997; Waxman 1997; Katz & Piran 1997; Panaitescu et al. 1997; Tavani 1997), but these studies treat a blast wave scenario, whereas we consider highly collimated outflows. This significantly reduces the energetics requirements and the need for the emitting region to be radiatively efficient. Indeed, we do not find that the radiating plasmoid in our model for GRB 970508 slows to nonrelativistic speeds.

The small beaming angles and large Lorentz factors derived here have important implications for GRB models under the assumption that the prompt gamma-ray emission from a typical GRB has a beaming angle $\theta_{\text{GRB}} \simeq 1/\Gamma_0$. This assumption is reasonable because there is no evidence from GRB light curves for spreading of the pulse widths during the main portion of the burst, which would be expected if the emitting plasma was significantly decelerating during the

gamma-ray active phase. We find that the inferred total gamma-ray energy for GRB 970508 is reduced by a factor $\sim 10^3$ from the isotropic value if the gamma-ray beaming pattern is $\propto \mathcal{D}_0^{3+\alpha}$, noting also that the gamma-ray emission is being viewed at an angle $\theta \approx 2.6/\Gamma_0$ from the beaming axis. Furthermore, because the gamma-rays are beamed into a fraction $\sim 1/(2\Gamma_0^2)$ of the full sky, a much larger source rate than the isotropic rate is required. This rate is too large to be accounted for by the rate of coalescing compact objects (see review by Dermer & Weiler 1995). If this model is correct, it therefore favors other GRB scenarios such as naked collapse events of white dwarfs (Dar et al. 1992), birth events of highly magnetized neutron stars (Usov 1992), or failed Type 1b supernova models (Woosley 1993). The large Lorentz factor found for the radio, optical and X-ray observations of GRB 970508 does not follow the power-law scaling (Paczynski & Rhoads 1993; Mészáros & Rees 1997) of the Lorentz factor with frequency invoked by Rhoads (1997) to estimate the optical transient detection rate. It also contradicts the inference by Rhoads (1997) that the material which produces the afterglow emission is only mildly relativistic, and thus removes a central motivation for the hypernova model of Paczynski (1997) insofar as highly collimated burst emission models are not ruled out.

If GRB 970508 is typical of a large fraction of GRBs and if the gamma-ray beaming pattern is indeed governed by the Doppler factor \mathcal{D}_0 at early times, then we can make definite predictions for the likelihood of detecting optical afterglow emission from such bursts. Figure 2 shows the afterglow light curves for our two sets of model parameters at different observing angles. For GRBs viewed at smaller angles than the inferred observing angle for GRB 970508 the afterglow optical flux is greatly enhanced, though the probability of detecting these bright afterglows is correspondingly smaller. For example, we find that the peak optical afterglow emission from one out of every ~ 25 GRBs will reach $R \simeq 13.3 + 5 \log(z/0.8)$, given that the peak R-band magnitude of GRB 970508 was 19.6 (Castro-Tirado et al. 1997). Optical transients not associated with GRBs (i.e., when $\theta \gg 1/\Gamma_0$) reach a much fainter peak magnitude. This effect is important for optical transient detection estimates and implies much lower rates than estimated by Rhoads (1997). As noted previously, the afterglow light curve (for the non-self-absorbed emission) should fall monotonically for observing angles $\theta < 1/\Gamma_0$. This can explain the optical afterglow light curve of GRB 920228 which appears to decline monotonically. The plasmoid producing the GRB 970508 optical afterglow between 3 and 10 days after the burst travels 30–100 pc. If it enters a lower density medium over this distance, its optical flux will decline much more slowly and could account for the discrepancy between the model fit and data shown in Figure 1a. This effect might also explain the flattening of the GRB 970228 R-band light curve after ~ 1 week (Galama et al. 1997a).

The burst afterglow model considered here is similar to nonthermal synchrotron models for the radio-through-optical continua of blazars, though with larger Lorentz factors. Hence, we expect that certain blazar characteristics should also be seen in GRB afterglows, such as superluminal motion and high polarization. In particular, we predict that radio and optical superluminal motion should be measured. From the parameters used to fit GRB 970508 we expect a motion of ~ 0.3 milliarcseconds per month. Detection of superluminal motion of this magnitude in afterglow

emissions of GRBs would require highly relativistic emission regions, in accord with the model proposed here.

This work was performed while J.C. held a National Research Council-NRL Research Associateship. C.D. acknowledges support by the Office of Naval Research.

REFERENCES

- Blumenthal, G. R. & Gould, R. J. 1970, *Rev. Mod. Phys.*, 42, 237
- Castro-Tirado, A. J., et al. 1997, *IAU Circ. No.* 6657
- Chevalier, C., & Ilovaisky, A. 1997, *IAU Circ. No.* 6663
- Dar, A., Kozlovsky, B. Z., Nussinov, S., & Ramaty, R. 1992, *ApJ*, 388, 164
- Dermer, C.D., & Weiler, T. J. 1995, *A&SS*, 231, 377
- Dermer, C.D., Sturmer, S. J., & Schlickeiser, R. 1997, *ApJS*, 109, 103
- Djorgovski, S. G., et al. 1997, *Nature*, 387, 876
- Fenimore, E., Madras, C. D., & Nayakshin, S. 1996, *ApJ*, 473, 998
- Fishman, G. & Meegan, C. 1995, *AARA*, 33, 415
- Frail, D., et al. 1997, *IAU Circ. No.* 6662
- Fruchter, A. et al. 1997, *IAU Circ. No.* 6674
- Galama, T. J., et al. 1997a, *Nature*, 387, 479
- Galama, T. J., et al. 1997b, *IAU Circ. No.* 6655
- Garcia, M., et al. 1997, *IAU Circ. No.* 6661
- Gould, R. J. 1979, *A&A*, 76, 306
- Groot, P. J., et al. 1997, *IAU Circ.* 6660
- Heise, J., 1997, presentation at 190th AAS meeting, Winston-Salem, NC, 32.02
- Katz, J. I., 1994, *ApJ*, 422, 248
- Katz, J. I., Piran, T., & Sari, R. 1997, *astro-ph/9703133*
- Katz, J. I. & Piran, T. 1997, *astro-ph/9706141*
- Kopylov, A. I., et al. 1997a, *IAU Circ. No.* 6663
- Kopylov, A. I., et al. 1997b, *IAU Circ. No.* 6671
- Mészáros, P., & Rees, M. J. 1997, *ApJ*, 476, 232
- Metzger, M. R., Cohen, J. G., Chaffee, F. H., & Blandford, R. D., 1997, *IAU Circ. No.* 6676

Metzger, M. R., et al. 1997, *Nature*, 387, 878
Mignoli, M., et al. 1997, *IAU Circ. No.* 6661
Paczyński, B., & Rhoads, J. E. 1993, *ApJ*, 418, L5
Paczyński, B. 1997, *astro-ph/9706232*
Panaitescu, A., Wen, L., Laguna, P., & Mészáros, P. 1997, *ApJ*, 482, 942
Piro, L., et al. 1997, *IAU Circ. No.* 6656
Rhoads, J. E. 1997, *astro-ph/9705163*
Ruffert, M., Janka, H.-T., Takahashi, K., & Schaefer, G. 1997, *A&A*, 319, 122
Schaefer, B., et al. 1997, *IAU Circ.* 6658
Tavani, M. 1997, *ApJ*, 483, L87
Usov, V. 1992, *Nature*, 357, 472
Waxman, E. 1997, *astro-ph/9705229*
Wijers, R. A. M. J., Rees, M. J., & Mészáros, P. 1997, *MNRAS*, 288, L51
Woosley, S. E., 1993, *ApJ*, 405, 273

Table 1: Decelerating Plasmoid Parameters for the Afterglow Lightcurves of GRB 970508

Model	Γ_0	θ ($^\circ$)	A_0 (cm^2)	ρ/m_p (cm^{-3})	v_{th} (cm s^{-1})	B_0 (G)	η
1	300	0.486	2.5×10^{31}	0.1	3×10^7	10^{-2}	0.02
2	500	0.310	4.0×10^{29}	1.0	1×10^7	10^{-3}	0.4

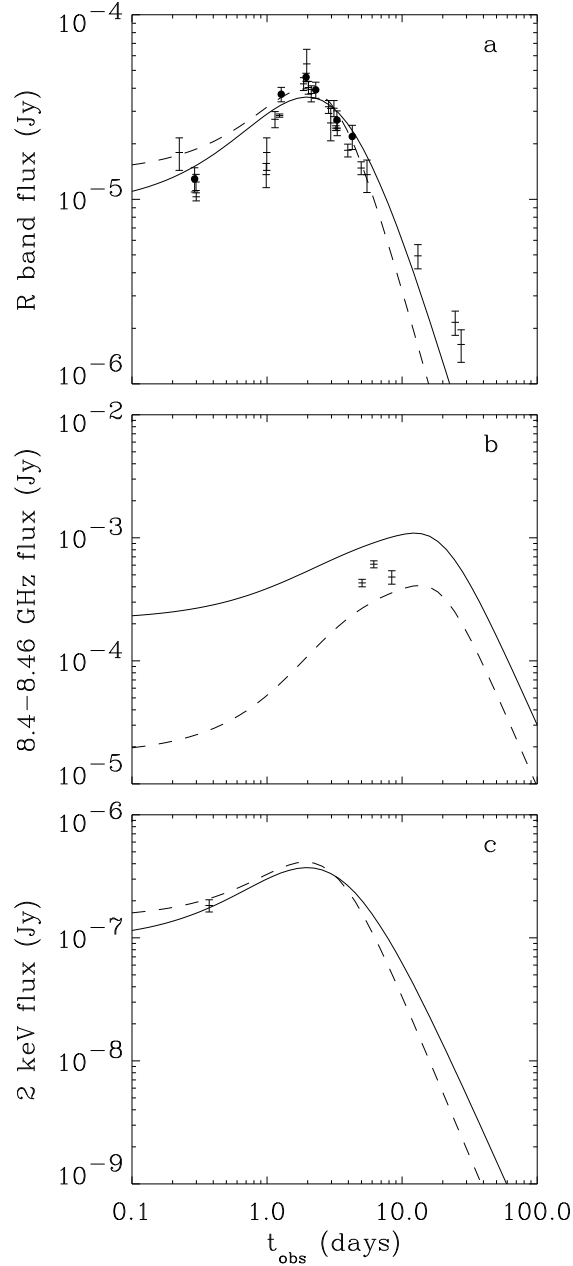


Fig. 1.— Optical, radio and X-ray light curves for the afterglow of GRB 970508. The R-band data from Djorgovski et al (1997) are plotted as filled circles and the remaining R-band data [from Galama et al. (1997b), Castro-Tirado et al. (1997), Schaefer et al. (1997), Groot et al. (1997), Garcia et al. (1997), Chevalier & Ilovaisky (1997), Kopylov et al. (1997a & b), Fruchter et al. (1997), and Metzger et al. (1997)] are scaled to the measurement of Mignoli et al. (1997) of $R = 19.78$ at May 10.85 which has been photometrically calibrated by Djorgovski et al.. The 8.4–8.64 GHz radio data are from Frail et al. (1997), and the 2 keV data point is from Piro et al. (1997). The solid curves are for the Model 1 parameters and the dashed curves are for Model 2. Note that the model X-ray light curves may also be affected by a high energy cut-off in the electron distribution.

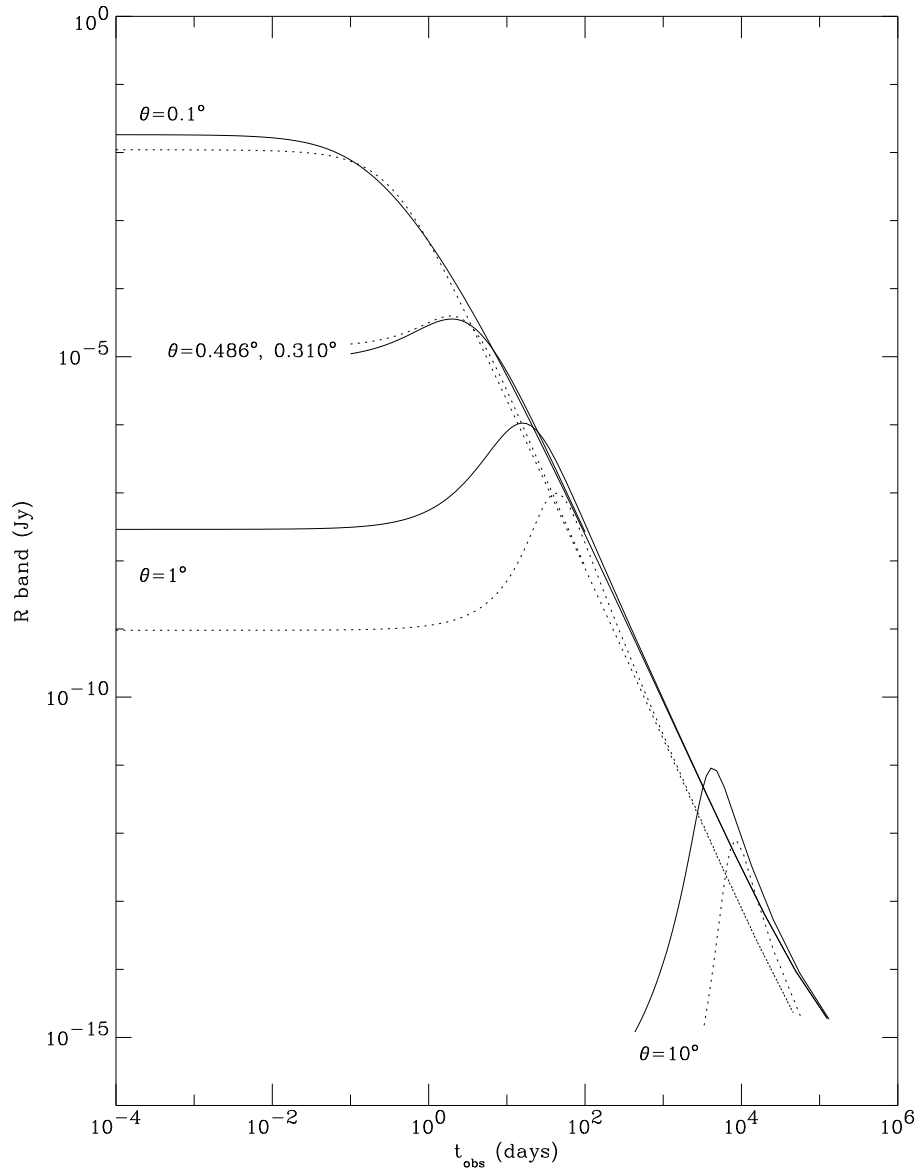


Fig. 2.— R-band light curves at various viewing angles for the two sets of model parameters, Model 1 (solid curve) and Model 2 (dotted).